analytical chemistry

pubs.acs.org/ac Article

Photoelectrochemical Biosensor for MicroRNA-21 Based on High Photocurrent of TiO_2/Two-Dimensional Coordination Polymer $CuCl_x(MBA)_y$ Photoelectrode

Jiao Yang, Yanzhou Li, Longhua Guo,* Bin Qiu,* and Zhenyu Lin*

Cite This: *Anal. Chem.* 2021, 93, 11010−11018 Read Online

ACCESS | Metrics & More | Article Recommendations | Supporting Information

ABSTRACT: Conventional photosensitive materials such as TiO_2 suffer from restricted absorption in the ultraviolet region, fast recombination of photogenerated electron−hole pairs, and a lack of functional groups for biocoupling, which hinder their application in photoelectrochemical (PEC) biosensing. Herein, a new coordination polymer (CP) based on Cu(I), chloridion, and 4-mercaptobenzoic acid (MBA) has been designed and synthesized (called $CuCl_x(MBA)_y$). The prepared p-type $CuCl_x(MBA)_y$ exhibits visible-light absorption due to its narrow optical band gap (2.59 eV), and its proper band edge position enables it to form a p−n junction with TiO_2. Through layer-by-layer assembling, the photocurrent intensity of the $CuCl_x(MBA)_y/TiO_2$/FTO composite photoelectrode was 3.7-fold higher than that of a TiO_2/FTO electrode and 35-fold higher than a $CuCl_x(MBA)_y$/FTO electrode. The potential enhancement mechanism was discussed, which lies in the contributions of $CuCl_x(MBA)_y$ in enhancing absorption in the visible-light region and boosting the separation of electron−hole pairs of TiO_2 by the p−n junction. Furthermore, $CuCl_x(MBA)_y$ nanosheets can realize bioconjugation directly, thanks to its abundant carboxyl groups. The $CuCl_x(MBA)_y/TiO_2$/FTO composite photoelectrodes were applied to develop a sensitive PEC biosensor for microRNA-21 (model target). By subtly exploiting the energy transfer between $CuCl_x(MBA)_y$ and Au nanoparticles (AuNPs), AuNPs served as effective quenchers. In the presence of the target, AuNP-labeled sDNA1 connected to the electrode surface, and thus, a decreased photocurrent was obtained. The proposed biosensor has a low detection limit of 0.29 fM (S/N = 3), good selectivity, and reproducibility. The proposed system was applied to monitor microRNA in cancer cells with satisfying results.

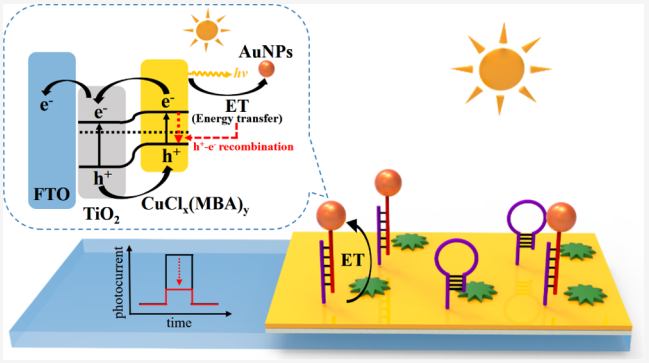

INTRODUCTION

Photoelectrochemical (PEC) detection technique has the advantages of simple equipment, low background, and high sensitivity.[1] TiO_2 is one of the most used n-type photoactive materials due to its low cost, low toxicity, and high chemical stability. However, the main drawbacks of TiO_2 for the application in biosensing are as follows: (i) the absorption of TiO_2 (band gap ~3.2 eV) is mainly restricted to the ultraviolet region (which accounts for only 3−5% in the full solar spectrum),[2−4] (ii) the fast recombination of photogenerated electron−hole pairs,[5,6] and (iii) the lack in eligible functional groups for biocoupling. Much effort has been made to overcome these limitations. First, to broaden the light absorption range, sensitizers, such as organic dyes and quantum dots, have been used to enhance light absorption in the visible range.[2,7,8] Second, fabricating heterojunctions has been proved to be one of the most promising ways to boost spatial separation of electron−hole pairs,[9] especially for p−n heterojunctions driven by the synergy between the internal electric field and the band alignment. The photogenerated electrons are transferred to the conduction band (CB) of the n-type semiconductors and the holes to the valence band (VB) of the p-type semiconductors, thus facilitating the spatial separation of electron−hole pairs and suppressing their recombination effectively.[9,10] Finally, to realize biosensing, TiO_2 often combines with other nanomaterials with eligible functional groups such as amino or carboxyl groups. However, capable nanomaterial which can effectively overcome these limitations of TiO_2 is not abundant. It is urgent but challenging to explore new nanomaterials to improve the performance of TiO_2 in the two or more aspects aforementioned.

Coordination polymers (CPs) have the advantages of simple synthetic routes and good electrical and optical properties.[11] By regulating the metal centers, ligands, or synthesis conditions, CPs with diverse structures, tunable electrical properties, and

Received: May 30, 2021
Accepted: July 20, 2021
Published: July 29, 2021

https://doi.org/10.1021/acs.analchem.1c02267
Anal. Chem. 2021, 93, 11010−11018

good optical performance can be obtained,[12,13] and abundant functional groups for biocoupling can be realized easily.[14,15] For example, Li and co-workers synthesized a series of metal−organic chalcogenides by using different metal ions (Cu^+, Ag^+, and Au^+) and changing the functional groups of the ligand (−COOH, −F, $-OCH_3$, −OH, or $-NH_2$). The prepared two-dimensional (2D) CPs exhibited regulable conductivity, widely tunable optical band gaps, and light absorption range, as well as diverse functional groups,[14] which make CPs promising candidates for overcoming the aforementioned drawbacks of TiO_2. Actually, CPs have been used to develop PEC sensors recently, but till now, most applications of CPs in PEC biosensors have only focused on their physical properties, such as apertures, large surface area, and adsorption capacity. For example, Wang and co-workers took the advantage of the large surface area and high porosities of UiO-66, loading a large number of photoactive dyes $[Ru(bpy)_3]^{2+}$,[16] which increased the photocurrent significantly; Zhan and co-workers fabricated ZnO@ZIF-8 nanorods, achieving a high selectivity toward molecules in different sizes thanks to the limitation of the aperture of the ZIF-8 shell.[17] However, the advantages of the tunable band gap, light-absorption range, proper band edge position, and abundant functional groups have not been fully applied.

Herein, using Cu(I) as the metal center and 4-mercaptobenzoic acid (MBA) and chloridion as the ligands, new 2D CP (called $CuCl_x(MBA)_y$) nanosheets have been designed and synthesized. First, the yellow $CuCl_x(MBA)_y$ nanosheets have a narrow optical band gap (2.59 eV) and have visible-light absorption. Second, primary characterization indicated that the p-type $CuCl_x(MBA)_y$ exhibited a proper band edge position which can form p−n junction with TiO_2. Moreover, $CuCl_x(MBA)_y$ nanosheets have abundant carboxyl groups which can realize bioconjunction easily. By sample layer-by-layer assembling on the electrode surface, $CuCl_x(MBA)_y$ can significantly enhance the photocurrent of TiO_2 by extending light absorption to the visible region and boosting the separation of electron−hole pairs by the p−n junction. The prepared $CuCl_x(MBA)_y/TiO_2$/FTO electrodes were applied to develop a sensitive PEC biosensor for microRNA-21 (model target) using Au nanoparticles (AuNPs) as quenchers through the energy-transfer (ET) process,[18−20] and an amplification strategy based on the Nb.BbvCI enzyme was coupled to enhance the sensitivity. In the presence of the target, many AuNP-labeled sDNA1 connected to the electrode surface, so a decreased photocurrent was detected. The photocurrent intensity has a good linear relationship with the logarithm of the target concentration from 0.5 fM to 1.0 nM with a low detection limit of 0.29 fM (S/N = 3), and the biosensor has good performance in selectivity, reproducibility, and real sample analysis.

EXPERIMENTAL SECTION

Chemicals and Reagents. Titanium dioxide (TiO_2), copper(I)oxide (Cu_2O), *N*-hydroxysuccinimide (NHS), 1-ethyl-3-(3-dimethylaminopropyl)-carbodiimide hydrochloride (EDC), sodium borohydride ($NaBH_4$), and bovine serum albumin (BSA) were purchased from Aladdin Bio-Chem Technology Co., Ltd. (Shanghai China). MBA (90%) was purchased from Adamas Reagent, Ltd. (Shanghai China). Chloroauric acid tetrahydrate ($HAuCl_4{\cdot}4H_2O$), ethanol (AR, ≥99.7%), and hydrochloric acid (HCl, 36−38%) were purchased from Sinopharm Chemical Reagent Co., Ltd. (China). Nicking endonuclease Nb. BbvCI and 10× NEBuffer buffer were purchased from New England Biolabs (Beijing, China). All chemical reagents were of analytical grade, and all aqueous solutions were prepared with Milli-Q water (18.2 MΩ·cm). High-performance liquid chromatography (HPLC)-purified DNA were purchased from Shanghai Sangon Biotechnology Co., Ltd. (Shanghai, China). HPLC-purified microRNAs were obtained from the Takara Biotechnology Co., Ltd. (Dalian, China). All microRNA-relevant processes were under the protection of RNase inhibitor. The sequences are shown in the Supporting Information. Buffer solutions used in this work were 10 mM phosphate buffer saline (PBS, pH 7.4), 1× TE buffer (containing 10 mM Tris-HCl, 1 mM EDTA), DNA hybridization buffer (containing 1× TE, 1 M NaCl, and 0.2 mM $MgCl_2$; pH 7.0), and 1× NEBuffer 2 (containing 10 mM Tris-HCl, 1 mM DTT, 50 mM NaCl, and 10 mM $MgCl_2$; pH 7.9).

Apparatus. Transmission electron microscopy (TEM) images were obtained using an HT7700 TEM instrument (Hitachi, Japan). Atomic force microscopy (AFM) measurements were performed using a Bruker dimension ICON scanning probe microscope. Fourier-transform infrared (FTIR) spectra were recorded using a Nicolet-6700 spectrometer (Thermo Scientific, USA). UV−vis absorption spectra were obtained with a UV-2310 UV−vis−NIR spectrophotometer (Tianmei, China). X-ray diffraction (XRD) patterns were recorded by a D8 Advance X-ray diffractometer (Bruker, Germany) using Cu Kα radiation (λ = 1.5418 Å). Fluorescence spectra were recorded by an F-4600 fluorescence spectrophotometer (Hitachi, Japan) equipped with a xenon lamp. X-ray photoelectron spectroscopy (XPS) was conducted by a Thermo Scientific ESCALAB 250 Xi XPS system. UV−vis diffuse reflection spectroscopy (UV−vis DRS) was performed with a Varian Cary 5000 Scan UV−vis−NIR spectrophotometer using $BaSO_4$ in a quartz plate as a reference. PEC measurements were carried out using a homemade PEC system. A 300 W Xe lamp (the light intensity was about 800 mW/cm^2) was used as the light source. Ag/AgCl (KCl-saturated) electrode worked as the reference electrode; FTO electrode with a fixed valid area of 0.3 cm^2 served as the working electrode, and Pt wire acted as the counter electrode. The photocurrent was recorded by a CHI660D electrochemical workstation (Shanghai Chenhua, China) with a bias voltage of 0.5 V, and 10 mM PBS was used as the base solution for PEC tests.

Synthesis of $CuCl_x(MBA)_y$ Nanosheets. Briefly, 0.15 g of MBA powder and 5 mL of C_2H_5OH were added into a 10 mL vial, then 120 μL of HCl (36−38%) and 0.025 g of Cu_2O powder were added, respectively, followed by ultrasound for 30 min. Next, the vial with the mixture was shifted to an oven, and the temperature was kept at 85 °C for 3 days. The resultant bright-yellow sediment was centrifuged and washed by C_2H_5OH and deionized water (DI water) 3 times. Finally, $CuCl_x(MBA)_y$ nanosheets were obtained after vacuum drying at 85 °C.

Synthesis of AuNPs. The preparation of AuNPs was according to previously reported methods.[18,20] Typically, AuNPs were prepared by the reduction of $HAuCl_4$ (20 mL, 0.25 mM) with freshly prepared ice-cold $NaBH_4$ (0.6 mL, 100 mM); under vigorous stirring, the mixed solution turned to orange-red and after stirring in the ice bath for 10 min and for another 3 h at room temperature, the solution changed to wine; the obtained solution was stored at 4 °C for further use.

Signal Amplification Strategy Based on Nicking Enzyme Nb.BbvCI. The thiolated HP2 was treated with

https://doi.org/10.1021/acs.analchem.1c02267
Anal. Chem. 2021, 93, 11010−11018

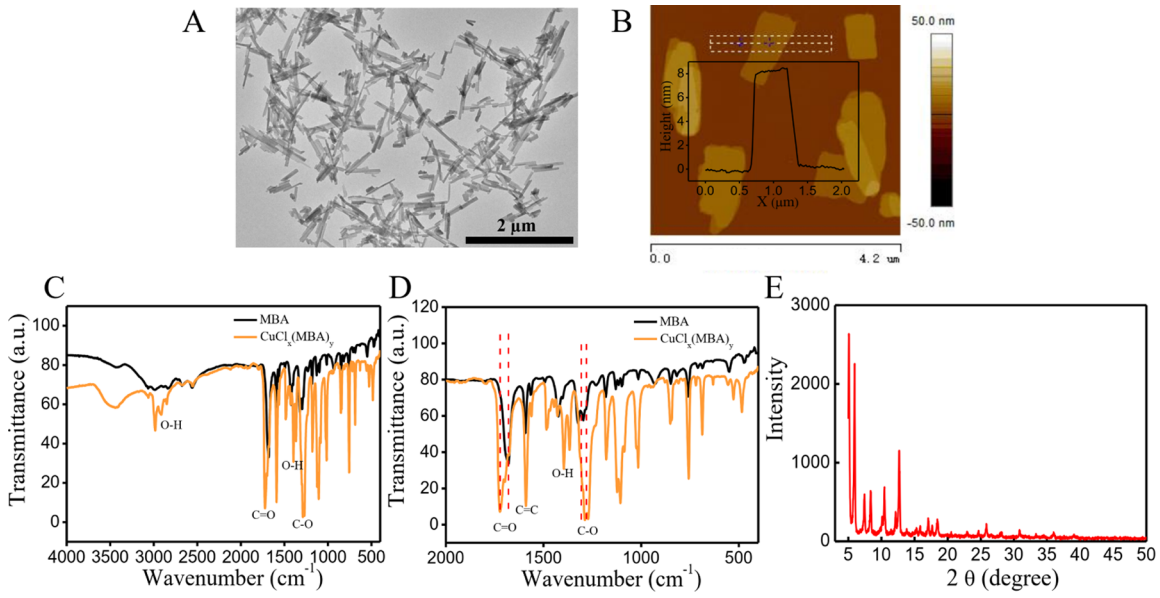

Figure 1. (A) TEM and (B) AFM images of the $CuCl_x(MBA)_y$ nanosheets. (C) FTIR spectra of the $CuCl_x(MBA)_y$ nanosheets and MBA. (D) Partial enlarged view of FTIR spectra of the $CuCl_x(MBA)_y$ nanosheets and MBA. (E) PXRD patterns of $CuCl_x(MBA)_y$ nanosheets.

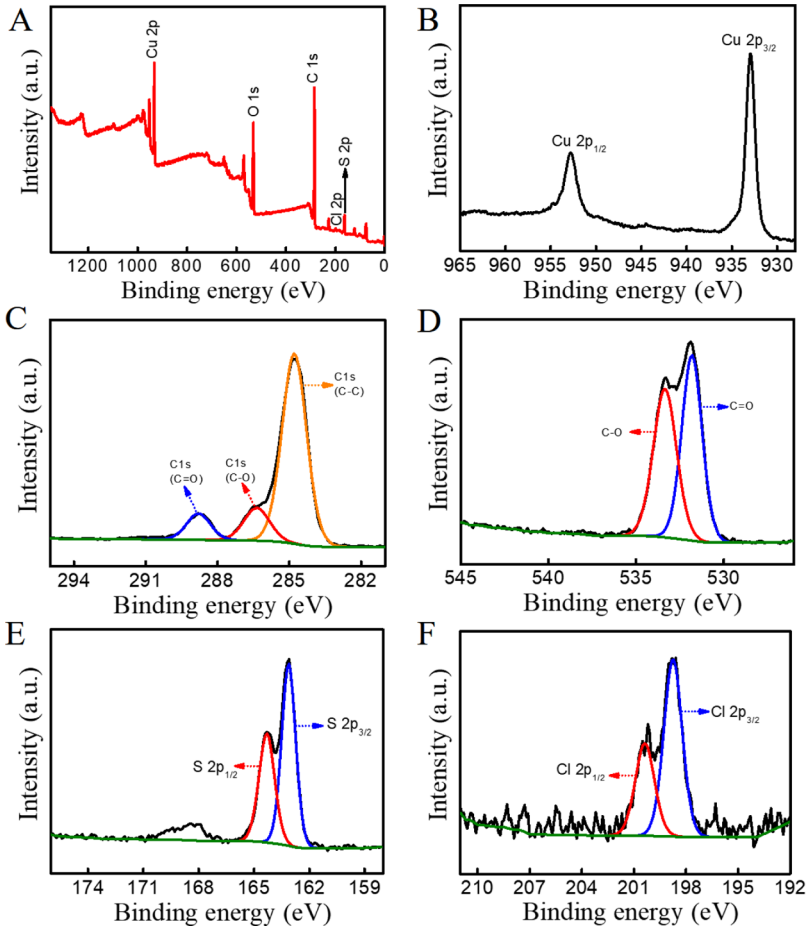

Figure 2. (A) XPS survey spectrum and HR-XPS spectra of (B) Cu, (C) C, (D) O, (E) S, and (F) Cl (the background at 284.8 eV was used as the internal standard).

TCEP to reduce the disulfide bond before use. Afterward, 40 μL of 2.5 μM HP2, 40 μL of 2.5 μM assistant probes, and 20 μL of samples containing the target in different concentrations were mixed. Then, 10 U of nicking enzymes Nb.BbvCI and 10 μL of 1× NEBuffer buffer were added, and the mixture was incubated at 37 °C for 50 min to generate massive sDNA1. Subsequently, the mixture was heated to 80 °C and keep for 20 min to

https://doi.org/10.1021/acs.analchem.1c02267
Anal. Chem. 2021, 93, 11010−11018

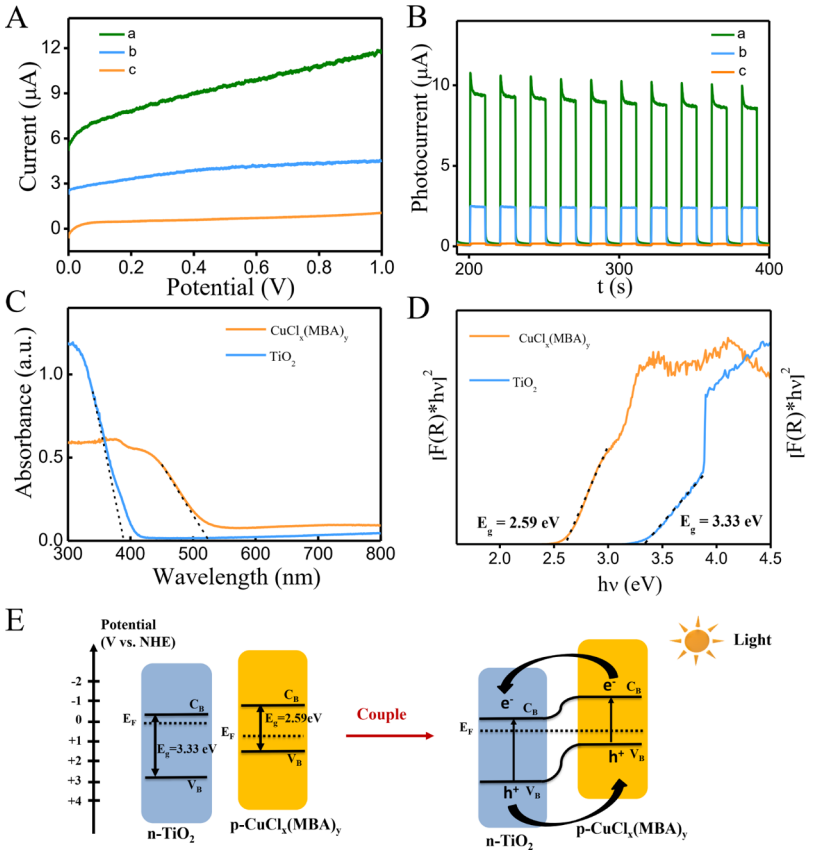

Figure 3. (A) *I*−*V* curve under illumination of (a) $CuCl_x(MBA)_y/TiO_2$/FTO electrode, (b) TiO_2/FTO electrode, and (c) $CuCl_x(MBA)_y$/FTO electrode in 10 mM PBS from 0 to 1.0 V. (B) PEC tests of (a) $CuCl_x(MBA)_y/TiO_2$/FTO electrode, (b) TiO_2/FTO electrode, and (c) $CuCl_x(MBA)_y$/FTO electrode in 10 mM PBS when the working potential was 0.5 V. (C,D) UV−vis diffuse reflectance spectra of TiO_2 and $CuCl_x(MBA)_y$. (E) Band alignment diagram between TiO_2 and $CuCl_x(MBA)_y$ before and after the formation of the p−n junction. The concentrations of TiO_2 and $CuCl_x(MBA)_y$ were 1.5 mg/mL for electrode modification.

deactivate the nicking enzyme, then cooled naturally to room temperature, and the final solution was stored at 4 °C.

Synthesis of sDNA1-AuNPs. 100 μL of AuNP solution (containing 50 mM NaCl) was added to the resultant solution of enzyme-mediated amplification, followed by gently shaking for 10 h in a dark environment. The sDNA1-AuNPs were purified twice by centrifugation and redistributed in a buffer and stored at 4 °C for further use.

Construction of the Biosensor. First, the FTO electrodes were washed by ethanol, acetone, and DI water, respectively, and then dried in air. 10 μL of 2.0 mg/mL TiO_2 solution was dropped to the clean FTO electrodes on the fixed electrode area of 0.3 cm^2; afterward, it was calcined at 450 °C for 60 min after drying in the air. Next, 10 μL of 2.0 mg/mL $CuCl_x(MBA)_y$ nanosheets in 0.1% Nafion solution was dropped to the TiO_2-modified electrodes and then dried in the air to form a composite photoelectrode. Then, the $TiO_2/CuCl_x(MBA)_y$-modified electrodes were immersed in a 2.0 μM HP1 solution containing 20 mg/mL EDC and 10 mg/mL NHS for 2 h at 37 °C to realize the condensation reaction between the carboxyl group of $CuCl_x(MBA)_y$ nanosheets and amidogen of HP1, which were immobilized on the electrode surface and served as capture probes. Whereafter, the $TiO_2/CuCl_x(MBA)_y$/HP1-modified electrodes were immersed in sDNA1-AuNPs solution prepared by samples containing the target in different concentrations, respectively. Finally, the $TiO_2/CuCl_x(MBA)_y$/HP1/sDNA1-AuNP-modified electrodes were washed by DI water gently and immersed in 10 mM PBS for the PEC test.

RESULTS AND DISCUSSION

Characterization of $CuCl_x(MBA)_y$. The TEM image (Figure 1A) shows $CuCl_x(MBA)_y$ as rectangular nanosheets which had a uniform morphology; the length of the rectangular nanosheets was 500 nm to 1.0 μm, and the width was 100 to 150 nm. The AFM image of the $CuCl_x(MBA)_y$ nanosheets is displayed in Figure 1B; the thickness of the nanosheets was about 8 nm, and the morphology was consistent with that in Figure 1A. The FTIR spectra of the ligand (MBA) and the prepared nanosheets are shown in Figure 1C,D; an apparent absorption band of −OH stretching vibration at 3000−3430 cm^{-1} can be observed. The absorption peaks at 1680 and 1274 cm^{-1} originated from the C═O group and −COO groups of MBA, respectively, while the absorption peak of C═O groups of $CuCl_x(MBA)_y$ appeared at 1680 and 1724 cm^{-1}, and the absorption peak of −COO groups of $CuCl_x(MBA)_y$ shifted to 1308 cm^{-1}. The peak shift of $CuCl_x(MBA)_y$ compared to MBA may be due to two reasons. First, after the coordination reaction, the electron density of the carboxylic carbon atom changed, which indicated the occurrence of the coordination reaction. Second, a little MBA maybe esterify with C_2H_5OH during the solvothermal reaction. The abundant carboxyl groups of the $CuCl_x(MBA)_y$ nanosheets can be verified by the obvious absorption of the C═O group at 1680 cm^{-1} and the absorption peak of −OH at 3000−3430 and 1395 cm^{-1}. As shown in Figure S1 (in the Supporting Information), the $CuCl_x(MBA)_y$ nanosheets showed a negative potential of −24.5 mV, which

https://doi.org/10.1021/acs.analchem.1c02267
Anal. Chem. 2021, 93, 11010−11018

Scheme 1. Principle of the Proposed PEC Sensor

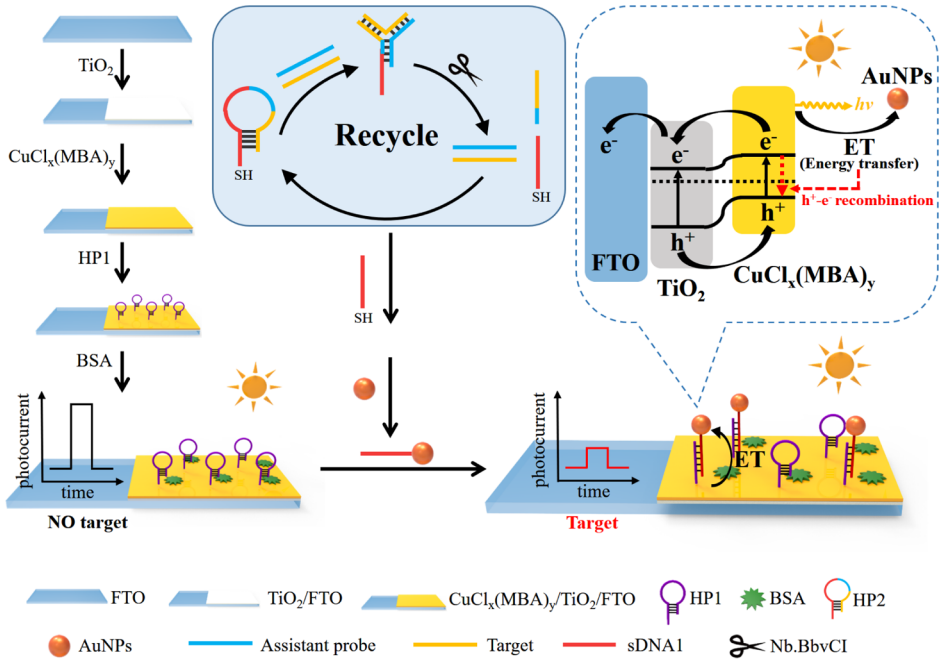

was also attributed to the carboxyl groups. As illustrated in Figure 1E, the powder XRD (PXRD) spectrum indicated that a highly crystalline $CuCl_x(MBA)_y$ was obtained. Figure S2 shows the fluorescence spectra of $CuCl_x(MBA)_y$, which presented a fluorescence emission peak at 625 nm when excited at 365 nm, and the inset pictures are the images of $CuCl_x(MBA)_y$ nanosheets in water under sunlight and a UV lamp (λ = 365 nm), respectively. The $CuCl_x(MBA)_y$ nanosheet solution was yellow and exhibited orange emission when excited at 365 nm.

The elemental composition of $CuCl_x(MBA)_y$ was analyzed by XPS. As shown in Figure 2A, all elements Cu, C, O, S, and Cl were noticeable in the XPS survey spectra. High-resolution XPS (HR-XPS) spectra of Cu 2p (Figure 2B) displayed a characteristic peak of Cu(I) at 933.0 and 952.8 eV, corresponding to Cu $2p_{3/2}$ and Cu $2p_{1/2}$, respectively, indicating that the valence of Cu is monovalence. HR-XPS of C 1s (Figure 2C) showed the peaks of C−O (286.3 eV), C═O (288.7 eV), and C−C (284.8 eV). O 1s (Figure 2D) was assigned to C═O (531.8 eV) and C−O (533.3 eV), indicating the abundant carboxyl groups of the $CuCl_x(MBA)_y$ nanosheets. Figure 2E shows the HR-XPS of S 2p (163.1 and 164.2 eV), corresponding to S $2p_{3/2}$ and S $2p_{1/2}$, respectively. Figure 2F shows Cl 2p (198.6 and 200.2 eV), corresponding to Cl $2p_{3/2}$ and Cl $2p_{1/2}$, respectively. These results suggested the high degree of complexation of Cu(I), thiol groups of MBA, and chloridion. In conjunction with the TEM and FTIR measurements, the formation of the 2D $CuCl_x(MBA)_y$ nanosheets can be verified.

Mechanism of the Enhancement of Photocurrent Intensity. The SEM image of the TiO_2-modified FTO electrode (Figure S3A in the Supporting Information) showed the TiO_2 layer attached uniformly on the electrode surface, and the thickness was about 800 nm. The SEM image of the $CuCl_x(MBA)_y/TiO_2$-modified FTO electrode (Figure S3B in the Supporting Information) showed that the $CuCl_x(MBA)_y$ layer covered the TiO_2 layer evenly, and the thickness was about 1.3 μm. These results showed the uniform layer-by-layer modification, and there was good contact between $CuCl_x(MBA)_y$ and TiO_2. Then, the photocurrent responses of different electrodes were investigated. $I-V$ tests under illumination were carried out, and the results are displayed in Figure 3A The photocurrent increased with the increase in potential, and the photocurrent intensity of the $CuCl_x(MBA)_y/TiO_2$ composite photoelectrode enhanced obviously compared to that of the $CuCl_x(MBA)_y$- or TiO_2-modified electrodes. Moreover, when the potential was 0 V, the photocurrent of TiO_2 was positive, while that of $CuCl_x(MBA)_y$ was negative, which indicated that $CuCl_x(MBA)_y$ may be a p-type semiconductor, while TiO_2 is an n-type semiconductor. Figure 3B displays the photocurrents of different electrodes when the bias potential was 0.5 V after the formation of the composite photoelectrode (curve c); the photocurrent intensity was 3.7-fold higher than that of the bare TiO_2 (curve b) and 35-fold higher than that of $CuCl_x(MBA)_y$ alone (curve a). Since a higher potential will cause more substrate disturbance and a higher dark current, 0.5 V was chosen as the working potential.

To figure out the mechanism of photocurrent enhancement, a UV−vis diffuse reflectance test was carried out. As shown in Figure 3C, the absorption of $CuCl_x(MBA)_y$ had an obvious redshift compared with TiO_2, indicating a narrower bandgap and reduced energy of band-to-band photon excitation. Figure 3D presents the reflectance of TiO_2 and $CuCl_x(MBA)_y$ nanosheets, which was measured using the diffuse reflectance method.[21,22] The band gap was estimated by the Tauc relation $(F(R)h\nu)^n = A(h\nu - E_g)$, where h is the Planck's constant, ν is the photon's frequency, A is a proportionality constant, the exponent n specifies the type of the electronic transitions, 2 for direct and 0.5 for indirect interband transitions (take n = 2 for $CuCl_x(MBA)_y$), and $F(R)$ is the Kubelka−Munk (K−M) function, and the equation is

$$\frac{K}{S} = F(R) = \frac{(1-R)^2}{2R}$$

in which K is the absorption coefficient, S is a scattering factor, and R is the reflectance.[23] Thus, the band gap of TiO_2 was estimated to be 3.33 eV, while the band gap of $CuCl_x(MBA)_y$

https://doi.org/10.1021/acs.analchem.1c02267
Anal. Chem. 2021, 93, 11010−11018

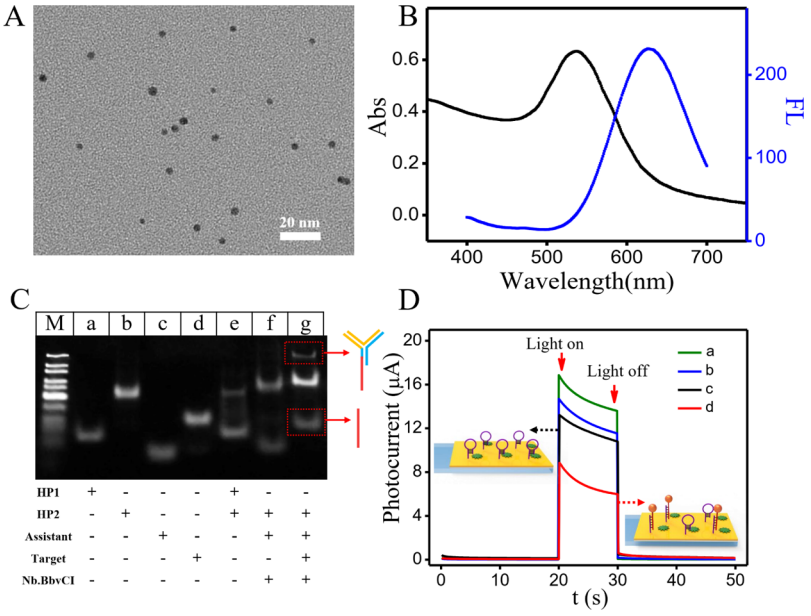

Figure 4. (A)TEM image of AuNPs. (B) UV−vis absorption spectrum of the AuNPs (black curve) and fluorescence spectra of the $CuCl_x(MBA)_y$ nanosheets (blue curve), λ_{ex} = 365 nm. (C) Gel electrophoresis image of the marker and 2.0 μM HP1 (lane a), 2.0 μM HP2 (lane b), 5.0 μM assistant probe (lane c), 5.0 μM target (lane d), 2.0 μM HP1 + 2.0 μM HP2 (lane e), 2.0 μM HP2 + 2.0 μM assistant probe + 0.5 U Nb.BbvCI nicking enzyme (lane f), and 2.0 μM HP2 + 2.0 μM assistant probe + 2.0 μM target + 0.5 U Nb.BbvCI nicking enzyme (lane g). (D) PEC response from different electrodes: (a) $CuCl_x(MBA)_y/TiO_2$/FTO electrode; (b) HP1/$CuCl_x(MBA)_y/TiO_2$/FTO electrode; (c) BSA/HP1/$CuCl_x(MBA)_y/TiO_2$/FTO electrode; and (d) sDNA1-AuNPs/BSA/HP1/$CuCl_x(MBA)_y/TiO_2$/FTO electrode (In 10 mM PBS when the potential was 0.5 V, the concentrations of TiO_2 and $CuCl_x(MBA)_y$ were 2.0 mg/mL for electrode modification.).

was estimated to be 2.59 eV, which verified that $CuCl_x(MBA)_y$ had a narrow band gap compared to TiO_2.

In order to figure out the band alignment between TiO_2 and $CuCl_x(MBA)_y$, ultraviolet photoelectron spectroscopy (UPS) measurements were carried out. As displayed in Figure S4 in the Supporting Information, the value of the Fermi level (E_f) for $CuCl_x(MBA)_y$ was 5.16 eV *versus* vacuum energy (E_{vac}), which was calculated by UPS work function from excitation energy (HeI, 21.2 eV), and that for the VB edge (E_{vb}) was 6.23 eV *versus* E_{vac}. Furthermore, the CB energy (E_{cb}) was determined to be 3.64 eV *versus* E_{vac} from $E_{vb} - E_g$. The values of E_F, E_{vb}, and E_{cb} were corresponding to 0.71, 1.78, and −0.81 eV *versus* RHE, respectively. Moreover, the Fermi level of $CuCl_x(MBA)_y$ deviated from the middle of the band gap and was close to the VB, which suggested that $CuCl_x(MBA)_y$ was a p-type 2D material, which confirmed the conjecture in the $I-V$ tests. Figure 3E shows the energy bands of the n-type TiO_2 and p-type $CuCl_x(MBA)_y$ before and after the formation of the p−n junction; the coupling caused the ascent of the Fermi level and energy band of $CuCl_x(MBA)_y$, while a decline of those of TiO_2 to equilibrate their Fermi levels. Upon irradiation, the separation of electron−hole pairs were induced; the p−n junction would then facilitate the fast transportation of these photogenerated excitons. The photoelectrons of $CuCl_x(MBA)_y$ injected into the CB of TiO_2 quickly, and the holes of TiO_2 migrated to the VB of $CuCl_x(MBA)_y$, which boosted the charge transfer significantly and enhanced the photocurrent intensity. Consequently, the composite photoelectrode with improved PEC performance was contributed to the enhanced charge separation by the p−n junction and the enhanced light-harvesting range by $CuCl_x(MBA)_y$.

Principle of the Proposed PEC Biosensor for microRNA-21. As shown in Scheme 1, after the modification of TiO_2 on the electrode surface, the solution of $CuCl_x(MBA)_y$ nanosheets rich in carboxyl groups was subsequently dropped to form a p−n junction. Afterward, amino-modified HP1 serving as a capture probe was modified on the electrode surface by connecting with the $CuCl_x(MBA)_y$ nanosheets through a condensation reaction between amino and carboxyl groups. In the presence of the target, HP2, the assistant probes and the target formed a Y-shaped junction structure, containing the nicking site of Nb.BbvCI enzyme; the Y-shaped junction structure was nicked by the Nb.BbvCI enzyme to produce sDNA1, and the assistant probe and the target were released to combine with another HP2 to form a new Y-shaped junction structure, which was nicked by Nb.BbvCI again. Therefore, the signal amplification strategy based on the Nb.BbvCI enzyme was induced, and a lot of sDNA1 was obtained as output. The output sDNA1 was connected with AuNPs through a Au−S bond. Then, the prepared sDNA1-AuNPs connected to the electrode surface through hybridization with HP1 via the complementary base-pairing principle; consequently, the AuNPs on the electrode surface quenched the photocurrent through an ET process between the $CuCl_x(MBA)_y$ nanosheets and AuNPs, which facilitated the recombination of electron−hole pairs[18−20] so that a decreased photocurrent of the system could be detected. In the absence of the target, Y-shaped junction structures could not be formed, and HP1 was unable to hybridize HP2; therefore, the AuNPs were unable to connect to the electrode surface to quench the photocurrent response, and a larger photocurrent was detected. With the increase in the target, the quenching effect enlarged, and the photocurrent decreased accordingly. Based on this principle, a sensitive PEC sensor for microRNA can be developed.

Feasibility Test. First, AuNPs were characterized by TEM (Figure 4A), which showed a uniform size of about 5 nm. Figure 4B exhibits the overlap of the UV−vis absorption spectrum of AuNPs (black) and the fluorescence spectra of $CuCl_x(MBA)_y$

https://doi.org/10.1021/acs.analchem.1c02267
Anal. Chem. 2021, 93, 11010−11018

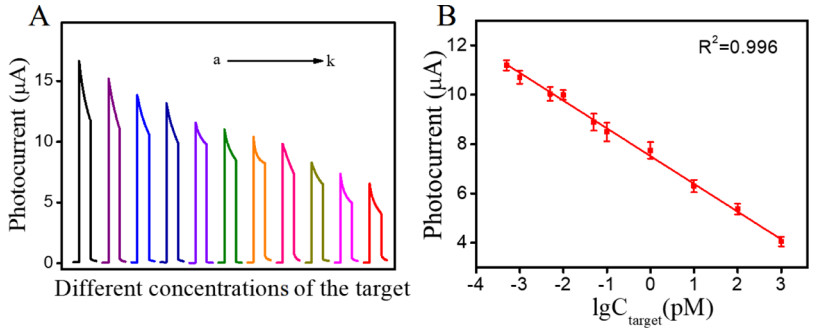

Figure 5. (A) PEC signal of the target at various concentrations, a to k: 0, 0.5, 1, 5, 10, 50, 100 fM, 1, 10, 100 pM, and 1 nM. (B) Linear plot of the PEC signal *vs* the logarithmic concentration of the target.

nanosheets (blue), which indicated that the ET phenomenon between the $CuCl_x(MBA)_y$ nanosheets and the AuNPs can take place. The polyacrylamide gel electrophoresis (12%) experiment was carried out to identify the Nb.BbvCI nicking enzyme-based signal amplification strategy (HP2 without AuNPs modified). As revealed in Figure 4C, lane e shows the bands of HP1 and HP2, indicating that HP1 cannot hybridize with HP2. Similarly, lane f shows that the assistant probe cannot hybridize with HP2 either, and there is no sDNA1 output with the Nb.BbvCI nicking enzyme in the absence of the target. Lane g displays the Y-shaped junction structure formed by HP2, assistant probe, and the target; with the help of the Nb.BbvCI nicking enzyme, a new band of output sDNA1 appeared, indicating the occurrence of Nb.BbvCI nicking enzyme-based signal amplification strategy in the presence of the target.

To verify the feasibility of the proposed PEC sensor to detect microRNA-21, first, the PEC response of different modification stages was tested. As displayed in Figure 4D, the prepared $CuCl_x(MBA)_y/TiO_2/FTO$ electrode exhibited a high photocurrent intensity (curve a). After modifying with HP1 (curve b) and blocking the nonspecific sites by BSA (curve c), the photocurrent response of the electrode decreased slightly because they impeded electron transfer due to their nonconducting property and steric hindrance effect. The surface density of the electrode-immobilized HP1 was measured by a chronocoulometric method and was calculated to be 1.282×10^{11} molecules/cm^{-2} (see details and Figure S5 in the Supporting Information).When modified with sDNA1-AuNPs (prepared when the concentration of target was 10 pM), the photocurrent of the system decreased greatly (curve d), indicating the feasibility of the proposed PEC sensor for the detection of the target.

Optimization of the Reaction Conditions. The concentration of TiO_2 was an important factor which affected the formation of the composite photoelectrode. The lack of TiO_2 may lead to the nonuniformity of the interface between TiO_2 and $CuCl_x(MBA)_y$ nanosheets, while the excessive TiO_2 would result in the increase in the thickness of the modified layer and hinder the electron transfer. Thus, the concentration of TiO_2 was optimized first, as shown in Figure S6A in the Supporting Information; the difference in the photocurrent between the control and experimental groups' Δphotocurrent (Δphotocurrent = $I_0 - I$, where I_0 is the photocurrent in the absence of the target, and I is the photocurrent in the presence of the 10 pM target) increased with the increasing of TiO_2 concentration and reached a maximum at the concentration of 2.0 mg/mL. Therefore, 2.0 mg/mL was chosen as the appropriate concentration of TiO_2.

In addition, sufficient capture probes ensured high capture efficiency, but excessive capture probes caused steric hindrance. As displayed in Figure S6B in the Supporting Information, with the increasing of the concentration of HP1, Δphotocurrent enlarged when the concentration of HP1 increased from 0.5 to 2.0 μM, and when the concentration was 2.0 μM, Δphotocurrent was maximized. Thus, 2.0 μM HP1 was chosen as the best concentration. The amplification strategy based on Nb.BbvCI digestion was vital for target detection; sufficient dosage and reaction time of Nb.BbvCI could ensure the digestion efficiency, while superfluous dosage and reaction time may cause nonspecific nicking, so the two factors were optimized. As illustrated in Figure S6C,D in the Supporting Information, Δphotocurrent increased with the increase in dosage and reaction time first and reached plateaus when the dosage was 10 U and reaction time was 50 min. Therefore, 10 U and 50 min were selected as the best conditions. Finally, enough incubation time of the electrode in the sDNA1-AuNPs solution was important, as displayed in Figure S6E in the Supporting Information, Δphotocurrent kept increasing and reached the maximum when the time was 120 min, indicating that 120 min was enough for incubation; hence, 120 min was chosen as the best condition.

Analytical Performance of the Biosensor. The analytical performance of the proposed sensing platform was assessed by detecting a series of samples containing various concentrations of microRNA-21 under the optimized conditions. As displayed in Figure 5A, with the increase in the target concentration (from a to k), the value of the photocurrent decreased synchronously. Figure 5B shows that there is a linear relationship between the photocurrent value (I) and the logarithmic concentration of the target from 0.5 fM to 1.0 nM. The linear equation could be expressed as follows

$$I(\mu A) = -1.125 \log C_{target}(pM) + 7.517 \quad (R^2 = 0.996)$$

where R is the correlation coefficient, and the limit of detection (LOD) is 0.29 fM (S/N = 3). The performance of the PEC sensor was compared with other methods for microRNA detection. As displayed in Table 1, the results indicated that the LOD and the wider linear range were superior to those described in previous studies.

Good selectivity and anti-interference are prerequisites for the practical application of biosensors; so, a selectivity test was carried out by utilizing several similar interferents. The concentration of the interferents was 50 pM, while the target concentration was 10 pM. As displayed in Figure S7A in the

https://doi.org/10.1021/acs.analchem.1c02267
Anal. Chem. 2021, 93, 11010−11018

Table 1. Comparison of the Developed PEC Sensors with Other Strategies for microRNA Detection

method	dynamic range	detection limit	references
fluorescent spectroscopy	0.1 pM to 10 nM	32 fM	24
electrochemical biosensor	5.0 fM to 50 pM	1.92 fM	25
electrochemiluminescence biosensor	1.0 fM to 10 pM	0.4 fM	26
PEC sensor	2.5 fM to 2.5 nM	0.83 fM	27
PEC sensor	0.2 pM to 25 nM	65 fM	28
PEC sensor	0.5 fM to 1.0 nM	0.29 fM	this work

Supporting Information, there was nearly no decrease in photocurrent intensity of interferents initially compared to that of the control. When all interferents were mixed with the target, the decrease in the photocurrent intensity was almost the same as that of the target alone initially. These results indicated the good selectivity and anti-interference of the proposed PEC sensor.

The reproducibility of the PEC sensor was assessed by five independent electrodes for a 10 pM target assessment. As illustrated in Figure S7B in the Supporting Information, the relative standard deviation was 3.2%, showing good reproducibility. Figure S7C in the Supporting Information shows the PEC test results in different matrixes; the test results in 10-fold diluted human serum were very close to that in 1× NEBuffer 2, showing the potential for target detection in a complex matrix. The long-term stability of the developed sensor was examined by storing the assembled sensor (the concentration of the target was 10 pM) in 1× NEBuffer 2 at 4 °C for 1 week; the test results showed no apparent change in the photocurrent response, indicating that the sensor had good stability.

Sample Determination. In order to evaluate the practical application capability of the proposed method, the PEC sensor was applied to detect cell lysates of MCF-7 (upregulated levels of microRNA-21) and HeLa (down-regulated levels of microRNA-21).[29] As displayed in Figure S7D in the Supporting Information, the rise of photocurrent was in accordance with the increased number of cells. The Δphotocurrent was enhanced slowly in the range of 10 to 10^4 cells in HeLa cell lysate, while the Δphotocurrent increased rapidly in MCF-7 cell lysate with the same cell number. The uptrend of the Δphotocurrent closely coincided with the increase in cell number and expression level, revealing that the proposed PEC sensor has the potential to monitor microRNA in cancer cells.

CONCLUSIONS

In summary, this study designed and synthesized new CPs $CuCl_x(MBA)_y$ based on Cu(I), MBA, and chloridion, which improved the PEC performance of TiO_2 in three aspects: first, due to the narrow optical band gap (2.59 eV) of $CuCl_x(MBA)_y$, the light absorption range was broadened to the visible region, which enhanced the light-harvesting efficiency. Second, the formation of a p−n junction facilitated the spatial separation of electron−hole pairs significantly, which increased the PEC response of TiO_2 obviously. Finally, the abundant carboxyl groups of $CuCl_x(MBA)_y$ realized biocoupling directly. This work applied a new and referable strategy for improving the performance of conventional photosensitive materials from different aspects. The biosensor based on the $CuCl_x(MBA)_y$ nanosheets had high sensitivity, good selectivity, reproducibility, and stability and also had the potential to monitor the target in cells. The combination of CPs and conventional inorganic photosensitive material provided a practical and efficient method for improving the performance of a sensing platform.

ASSOCIATED CONTENT

Supporting Information

The Supporting Information is available free of charge at https://pubs.acs.org/doi/10.1021/acs.analchem.1c02267.

Additional experiment details, cell culture and total microRNAs extraction, and synthetic oligonucleotide sequences; zeta potential, fluorescence, and UPS spectra for $CuCl_x(MBA)_y$; and SEM, chronocoulometric, optimization, selectivity, reproducibility, anti-interference performance, and real sample analysis for the sensor (PDF)

AUTHOR INFORMATION

Corresponding Authors

Longhua Guo − *College of Biological, Chemical Sciences and Engineering, Jiaxing University, Jiaxing, Zhejiang 314001, China*; Email: guolh@zjxu.edu.cn

Bin Qiu − *Ministry of Education Key Laboratory for Analytical Science of Food Safety and Biology, Fujian Provincial Key Laboratory of Analysis and Detection for Food Safety, College of Chemistry, Fuzhou University, Fuzhou, Fujian 350116, China*; Phone: 86-0591-22866135; Email: summer328cn@163.com

Zhenyu Lin − *Ministry of Education Key Laboratory for Analytical Science of Food Safety and Biology, Fujian Provincial Key Laboratory of Analysis and Detection for Food Safety, College of Chemistry, Fuzhou University, Fuzhou, Fujian 350116, China*; orcid.org/0000-0001-7890-6812; Phone: 86-0591-22866135; Email: zylin@fzu.edu.cn

Authors

Jiao Yang − *Ministry of Education Key Laboratory for Analytical Science of Food Safety and Biology, Fujian Provincial Key Laboratory of Analysis and Detection for Food Safety, College of Chemistry, Fuzhou University, Fuzhou, Fujian 350116, China*

Yanzhou Li − *Henan Key Laboratory of Polyoxometalate Chemistry, College of Chemistry and Chemical Engineering, Henan University, Kaifeng, Henan 475004, China*

Complete contact information is available at: https://pubs.acs.org/10.1021/acs.analchem.1c02267

Notes

The authors declare no competing financial interest.

ACKNOWLEDGMENTS

This project was financially supported by National Key Research and Development Program of China (no. 2019YFC1604701), National Sciences Foundation of China (21974020, 22001058) and the United Fujian Provincial Health and Education Project for Tackling the Key Research P. R. China (2019-WJ-11).

REFERENCES

(1) Zhao, W.-W.; Xu, J.-J.; Chen, H.-Y. *Chem. Rev.* **2014**, *114*, 7421−7441.

(2) Liu, X.-P.; Chen, J.-S.; Mao, C.-j.; Niu, H.-L.; Song, J.-M.; Jin, B.-K. *Biosens. Bioelectron.* **2018**, *116*, 23−29.

(3) Han, F.; Song, Z.; Nawaz, M. H.; Dai, M.; Han, D.; Han, L.; Fan, Y.; Xu, J.; Han, D.; Niu, L. *Anal. Chem.* **2019**, *91*, 10657−10662.
(4) Qin, X.; Wang, Q.; Geng, L.; Shu, X.; Wang, Y. *Talanta* **2019**, *197*, 28−35.
(5) Çakıroğlu, B.; Özacar, M. *Biosens. Bioelectron.* **2018**, *119*, 34−41.
(6) Wang, L.; Meng, Y.; Zhang, C.; Xiao, H.; Li, Y.; Tan, Y.; Xie, Q. *ACS Appl. Mater. Interfaces* **2019**, *11*, 9394−9404.
(7) Chen, J.; Kong, L.; Sun, X.; Feng, J.; Chen, Z.; Fan, D.; Wei, Q. *Biosens. Bioelectron.* **2018**, *117*, 340−346.
(8) Song, K.; Ding, C.; Zhang, B.; Chang, H.; Zhao, Z.; Wei, W.; Wang, J. *Microchim. Acta* **2018**, *185*, 310.
(9) Low, J.; Yu, J.; Jaroniec, M.; Wageh, S.; Al-Ghamdi, A. A. *Adv. Mater.* **2017**, *29*, 1601694.
(10) Wang, H.; Zhang, L.; Chen, Z.; Hu, J.; Li, S.; Wang, Z.; Liu, J.; Wang, X. *Chem. Soc. Rev.* **2014**, *43*, 5234−5244.
(11) Liu, J.-Q.; Luo, Z.-D.; Pan, Y.; Kumar Singh, A.; Trivedi, M.; Kumar, A. *Coord. Chem. Rev.* **2020**, *406*, 213145.
(12) Kaur, R.; Kim, K.-H.; Paul, A. K.; Deep, A. *J. Mater. Chem. A* **2016**, *4*, 3991−4002.
(13) Veselska, O.; Demessence, A. *Coord. Chem. Rev.* **2018**, *355*, 240−270.
(14) Li, Y.; Jiang, X.; Fu, Z.; Huang, Q.; Wang, G.-E.; Deng, W.-H.; Wang, C.; Li, Z.; Yin, W.; Chen, B.; Xu, G. *Nat. Commun.* **2020**, *11*, 261.
(15) Zhao, S.; Wang, Y.; Dong, J.; He, C.-T.; Yin, H.; An, P.; Zhao, K.; Zhang, X.; Gao, C.; Zhang, L.; Lv, J.; Wang, J.; Zhang, J.; Khattak, A. M.; Khan, N. A.; Wei, Z.; Zhang, J.; Liu, S.; Zhao, H.; Tang, Z. *Nat. Energy* **2016**, *1*, 16184.
(16) Wang, Z.; Yan, Z.; Wang, F.; Cai, J.; Guo, L.; Su, J.; Liu, Y. *Biosens. Bioelectron.* **2017**, *97*, 107−114.
(17) Zhan, W.-w.; Kuang, Q.; Zhou, J.-z.; Kong, X.-j.; Xie, Z.-x.; Zheng, L.-s. *J. Am. Chem. Soc.* **2013**, *135*, 1926−1933.
(18) Zhao, W.-W.; Wang, J.; Xu, J.-J.; Chen, H.-Y. *Chem. Commun.* **2011**, *47*, 10990−10992.
(19) Wen, G.; Dong, W.; Liu, B.; Li, Z.; Fan, L. *Biosens. Bioelectron.* **2018**, *117*, 91−96.
(20) Ma, Z.-Y.; Ruan, Y.-F.; Xu, F.; Zhao, W.-W.; Xu, J.-J.; Chen, H.-Y. *Anal. Chem.* **2016**, *88*, 3864−3871.
(21) Vargas, W. E.; Niklasson, G. A. *Appl. Opt.* **1997**, *36*, 5580−5586.
(22) Yang, L.; Miklavcic, S. J. *J. Opt. Soc. Am. A* **2005**, *22*, 1866−1873.
(23) Pathak, A.; Shen, J.-W.; Usman, M.; Wei, L.-F.; Mendiratta, S.; Chang, Y.-S.; Sainbileg, B.; Ngue, C.-M.; Chen, R.-S.; Hayashi, M.; Luo, T.-T.; Chen, F.-R.; Chen, K.-H.; Tseng, T.-W.; Chen, L.-C.; Lu, K.-L. *Nat. Commun.* **2019**, *10*, 1721.
(24) Yang, W.; Shen, Y.; Zhang, D.; Li, C.; Yuan, R.; Xu, W. *Anal. Chem.* **2019**, *91*, 7782−7789.
(25) Zhang, K.; Dong, H.; Dai, W.; Meng, X.; Lu, H.; Wu, T.; Zhang, X. *Anal. Chem.* **2017**, *89*, 648−655.
(26) Lu, H.-J.; Pan, J.-B.; Wang, Y.-Z.; Ji, S.-Y.; Zhao, W.; Luo, X.-L.; Xu, J.-J.; Chen, H.-Y. *Anal. Chem.* **2018**, *90*, 10434−10441.
(27) Xia, L. Y.; Zheng, Y. N.; Liang, W. B.; Li, M. J.; Hu, T.; Yuan, R.; Chai, Y. Q. *Chemistry* **2019**, *25*, 4087−4092.
(28) Song, X.; Hou, T.; Lu, F.; Wang, Y.; Liu, J.; Li, F. *Chem. Commun.* **2020**, *56*, 1811−1814.
(29) Jiang, X.; Wang, H.; Chai, Y.; Li, H.; Shi, W.; Yuan, R. *Anal. Chem.* **2019**, *91*, 10258−10265.

https://doi.org/10.1021/acs.analchem.1c02267
Anal. Chem. 2021, 93, 11010−11018